The Journal of Immunology

Discrete Event Modeling of CD4$^+$ Memory T Cell Generation

Martin S. Zand, Benjamin J. Briggs, Anirban Bose and Thuong Vo

J Immunol 2004; 173:3763-3772; ;
doi: 10.4049/jimmunol.173.6.3763
http://www.jimmunol.org/content/173/6/3763

The Journal of Immunology is published twice each month by
The American Association of Immunologists, Inc.,
1451 Rockville Pike, Suite 650, Rockville, MD 20852

Print ISSN: 0022-1767 Online ISSN: 1550-6606.

Discrete Event Modeling of CD4$^+$ Memory T Cell Generation[1]

Martin S. Zand,[2]* Benjamin J. Briggs,* Anirban Bose,* and Thuong Vo†

Studies of memory T cell differentiation are hampered by a lack of quantitative models to test hypotheses in silico before in vivo experimentation. We created a stochastic computer model of CD4$^+$ memory T cell generation that can simulate and track 10^1–10^8 individual lymphocytes over time. Parameters for the model were derived from experimental data using naive human CD4$^+$ T cells stimulated in vitro. Using discrete event computer simulation, we identified two key variables that heavily influence effector burst size and the persistent memory pool size: the cell cycle dependent probability of apoptosis, and the postactivation mitosis at which memory T cells emerge. Multiple simulations were performed and varying critical parameters permitted estimates of how sensitive the model was to changes in all of the model parameters. We then compared two hypotheses of CD4$^+$ memory T cell generation: maturation from activated naive to effector to memory cells (model I) vs direct progression from activated naive to memory cells (model II). We find that direct progression of naive to memory T cells does not explain published measurements of the memory cell mass unless postactivation expansion of the memory cell cohort occurs. We conclude that current models suggesting direct progression of activated naive cells to the persistent memory phenotype (model II) do not account for the experimentally measured size of the postactivation CD4$^+$, Ag-specific, memory T cell cohort. ***The Journal of Immunology*****, 2004, 173: 3763–3772.**

Quantitative models of cellular immune responses have permitted investigators to create experimentally testable hypotheses, which have often been counterintuitive, concerning fundamental lymphocyte processes (1). Such models have been used to predict B cell and TCR gene rearrangements (2), T cell population kinetics (3–5), the kinetics of HIV infection in CD4$^+$ T cell populations (6), and to compare hypotheses regarding B cell Ag receptor complex allelic exclusion (7). A significant drawback to many mathematical models of the immune system is that they do not treat individual cells as the fundamental unit of decision making (8), but rather rely on equations that reflect population behavior. Such approaches do not provide information about the behavior or possible molecular mechanisms behind the actions of individual lymphocytes.

To explore the kinetics of CD4$^+$ memory T cell emergence, we created a discrete event, stochastic computer model of immune activation. One advantage of discrete event modeling (DEM)[3] is that it may be used to track the properties of each individual "virtual lymphocyte" over time, a technique that is closer to the actual biology of memory T cell generation and can provide data similar to that derived from in vivo and in vitro experiments (9). This type of model uses random variation of key variables within predefined ranges and statistical distributions to explore the behavior of complex systems that are not easily studied using strict mathematical models (9).

Using DEM, we were able to simulate and track 10^1–10^8 individual CD4$^+$ lymphocytes from activation to memory cell emergence. T cell activation sets into motion two processes: the rapid expansion and subsequent contraction of a responder pool and the generation of a persistent memory cell pool. What is striking about this phenomenon is that the absolute number of T cells remains invariant, despite transient bursts of responder cell proliferation (10). Indeed, large fluctuations indicate serious defects in proliferation, apoptosis, or other regulatory pathways (11).

How does such tight regulation of the overall T cell mass occur? One possibility is that the immune system can sense the total T cell mass, and adjust proliferation and mitotic rates accordingly. Although such centralized planning may occur in the general sense, as in homeostatic proliferation (12), limiting the naive T cell mass (13, 14), and maintenance of CD8$^+$ memory cells (15), it is improbable that individual CD4$^+$ Ag-specific responses are controlled this way (16). The generation of persistent and specific T cell memory does not appear to be limited by global regulatory factors, but rather by decisions made by individual activated T cells and the escape of individual memory cells from apoptosis (17, 18).

Currently there are two major models for emergence of memory T cells, as elegantly explicated by Farber (19), with experimental data to support either model. Model I proposes that T cells progress from a naive state, become activated, and although most subsequently apoptose, a subset survive to become memory cells (20). In contrast, model II proposes that memory T cells are generated directly from the naive state, without traversing the effector state (17, 21, 22). In this report, we use discrete event simulation to compare these two hypotheses and their implications.

Materials and Methods

Computer modeling and statistical analysis

Computer modeling was performed using Extend (Version 5.04; Imagine That, San Jose, CA) Simulation Suite run on a Dell Optiplex GX400 computer (1.3 MHz, 386 MB RAM) under a Windows 2000 (Microsoft, Redmond WA) operating system. The simulation algorithm for this model is an iterative, branched and looped Markov chain implemented in a discrete event, time-based simulation environment. Extend uses a message-based architecture with an array data structure to track the 10^2–10^8 simulation items (lymphocytes) traveling through the model. Each virtual lymphocyte traverses a "flow chart" that is programmed via a graphical interface. At each stage the lymphocytes may have an action occur (divide, rest, change

*Nephrology Unit and †Department of Surgery, University of Rochester Medical Center, Rochester, NY 14642

Received for publication April 15, 2003. Accepted for publication July 6, 2004.

The costs of publication of this article were defrayed in part by the payment of page charges. This article must therefore be hereby marked *advertisement* in accordance with 18 U.S.C. Section 1734 solely to indicate this fact.

[1] This work is supported by National Institutes of Health Grant AI01641-05 (to M.S.Z.), and by the Vera and Edward Harris Family Foundation (to M.S.Z. and B.J.B.).

[2] Address correspondence and reprint requests to Dr. Martin S. Zand, Nephrology Unit, University of Rochester Medical Center, 601 Elmwood Avenue, Box 675, Rochester, NY 14642. E-mail address: martin_zand@urmc.rochester.edu

[3] Abbreviation used in this paper: DEM, discrete event modeling.

0022-1767/04/$02.00

surface markers, apoptose, etc.). Readers interested in a technical discussion of discrete event simulation are referred to excellent reviews of the algorithms (23) and their implementation in Extend (24). Simulation results reflect at least three separate runs for each data point.

Statistical analysis was performed using Statistica (StatSoft, Tulsa, OK). Gaussian curve-fitting of CDFSE; Molecular Probes, Eugene, OR) data was performed by exporting histogram data from Cytomation (Summit, Boulder, CO) to Statistica and using a quasi-Newtonian implementation of the least-squares regression algorithm for numerical curve fitting with the Kolmogorov-Smirnov test to assess goodness of fit.

Human subjects

Healthy volunteers both male and female and able to provide informed consent were recruited for phlebotomy. This study was approved by the University of Rochester Medical Center Human Subjects Review Board. The experimental protocol conforms to the Helsinki accords for human subjects. Research data were coded such that subjects could not be identified, directly or through linked identifiers, in compliance with the Department of Health and Human Services Regulations for the Protection of Human Subjects (45 CFR 46.101(b)(4)).

Monoclonal Abss and reagents

Lymphocytes were stimulated in flat-bottom 96-well plates coated for 1 h at 37°C with anti-CD3 (10 μg/ml, clone HIT3a; BD Pharmingen, San Diego, CA), anti-CD28 (10 μg/ml, clone CD28.2; BD Pharmingen) anti-human Abs. Labeling for flow cytometry was performed with the following mAbs purchased from BD Pharmingen: anti-CD4 (clone RPA-T4), anti-CD8 (clone HIT-8, CyChrome), and anti-CD25 (M-A251, CyChrome). Cell proliferation and viability reagents included: propidium iodide (Sigma-Aldrich, St. Louis, MO), TOPRO-3 (Molecular Probes), and CDFSE (Molecular Probes). Recombinant human IL-2 was purchased from R&D Systems (Minneapolis, MN).

Isolation of human lymphocytes

Human lymphocytes were isolated by Ficoll density gradient centrifugation from the peripheral blood of healthy volunteers. $CD4^+$ and $CD8^+$ responder cells were purified by negative selection using Ab-coupled (anti-human CD8, CD11b, CD16, CD19, CD36, and CD56) magnetic bead selection (Miltenyi Biotec, Auburn, CA). Isolated T cell subsets were verified to be 99% pure by flow cytometric analysis, and unactivated (data not shown). Cells were cultured at a density of 10^5 cells per 200-μl well in 96-well plates with DMEM supplemented with 10% heat-inactivated human AB serum, and 100 U/ml penicillin/streptomycin at 37°C in 100% humidity and 5% CO_2.

Cell cycle analysis

Cell cycle analysis was performed by CDFSE staining. Aliquots of 10^7 $CD4^+$ lymphocytes were incubated with 10 μm CDFSE (Molecular Probes) at room temperature for 8 min, followed by quenching with type Ab Rh^- human serum. Cells were washed and then cultured with 20 U/ml recombinant human IL-2 in wells that had been precoated for 1 h at room temperature with anti-CD3 (10 μg/ml) and anti-CD28 (10 μg/ml). At predetermined time points, viable cells were distinguished by exclusion of the fluorescent dye TOPRO-3 (Molecular Probes). Staining was analyzed by flow cytometry on a FACSCaliber dual laser cytometer (BD Biosciences, San Jose, CA) using CellQuest (BD Biosciences), WinMidi (Scripps, La-Hoya, CA), and Cytomation software (Summit).

Results

The model

Each stochastic, discrete event simulation of $CD4^+$ memory T cell generation begins with an initial number of "virtual" naive $CD4^+$ lymphocytes subject to an activation stimulus (Fig. 1). The events that follow are simulated for up to 400 h.[4] Each cell undergoes mitosis or apoptosis and has phenotypic markers that reflect its internal state (naive, activated, memory, anergic, or apoptotic).

The discrete event simulation is composed of several modules that correspond to the state transitions that a virtual lymphocyte undergoes: activation, commitment, mitosis, apoptosis, and persistent memory cells (Fig. 1). For all simulations, cells continue dividing until apoptosis or the transition to the persistent memory cell state occurs. For naive (Fig. 2*a*) and memory cells (Fig. 2*b*), the probability of apoptosis (P_{adeath}) increases with the number of prior mitoses the cell has undergone, as specified by an experimentally derived stochastic curve. For model I, maturation into a persistent memory cell occurs after a threshold of five prior mitoses (Fig. 2*c*). The time to complete cycling from G_0 through M is assigned to each cell before each mitotic event using an experimentally derived Gaussian distribution (Fig. 3, *d–f*). To compare sequential (model I) and direct (model II) memory cell progression, an alternative pathway was added to the model in which activated cells differentiate directly into memory cells and enter a persistent state (Fig. 1). In the following sections, we briefly review the derivation of critical data and assumptions used in the simulations, which are summarized in Table I.

T cell activation and commitment

We used data from several investigators indicating that 80–95% of murine $CD4^+$ lymphocytes activated with anti-CD3 in the presence of CD28 ligation, will up-regulate the IL-2R α-chain (activated dividing and activated quiescent subsets in the simulation), but only 60–80% undergo mitosis (5, 25, 26). We confirmed these data in human lymphocytes by activating naive $CD4^+$ T cells with solid phase anti-CD3, anti-CD28, and soluble IL-2 (20 U/ml), finding that 94 $\pm$ 4.2% of cells up-regulated $CD25^+$ at 25 h postactivation, but only 61 $\pm$ 7.1% subsequently entered into mitosis (data not shown). Thus, virtual lymphocytes in our simulation had a 95% chance of activation, and of those activated, 60% proliferated (activated-proliferating) and 40% did not (activated-anergic). We recognize that other variables, such as TCR signal strength (27), costimulation (5, 28), IL-2R signal strength (5), and preassembly of the CD3-TCR complex (29) affect activation frequencies, but chose this simplification as a starting point for simulations.

Activation delay period

We defined the activation delay as the lag time between TCR ligation with costimulation and completion of mitosis (Fig. 4*a*). Once TCR ligation occurs in the presence of the appropriate costimulatory signals, there is a delay of 48–72 h until the first mitosis occurs (25, 26, 30). Elegant studies by Iezzi et al. (31) have shown that for strong antigenic stimulation naive T cells require at least 14 h of Ag exposure for commitment to a robust proliferative response. Experiments with CDFSE-labeled murine T cells exposed to Ag indicate that the total delay (activation through completion of mitosis) is ~45–52 h under conditions of maximum costimulation with IL-2 supplementation (5, 32, 33). Progression from G_0 to S likely occurs 10–15 h before this time (34).

Several factors are known to modulate the activation delay. Different $CD4^+$ clonotypes exhibit heterogeneity with respect to triggering thresholds, largely as a function of TCR Ag affinity, Ag dose, and the presence of costimulatory signals (28). IL-2 increases the proportion of activated T cells progressing from G_0 to S phase, as does CD28 ligation (32–34). Although these factors are important for determining the magnitude of the responding $CD4^+$ T cell mass, our model has simplified this event to a single activation probability distribution reflecting this heterogeneity.

We measured the activation delay at maximal TCR stimulation and costimulation for naive human $CD4^+$ T cells activated with anti-CD3, anti-CD28, and IL-2 using two different methods: 1) breakpoint regression analysis of the mitotic index, and 2) Gaussian curve fitting as described by Gett and Hodgekin (5).

[4] A copy of the computer simulation for PC-based computers can be obtained from the corresponding author on request.

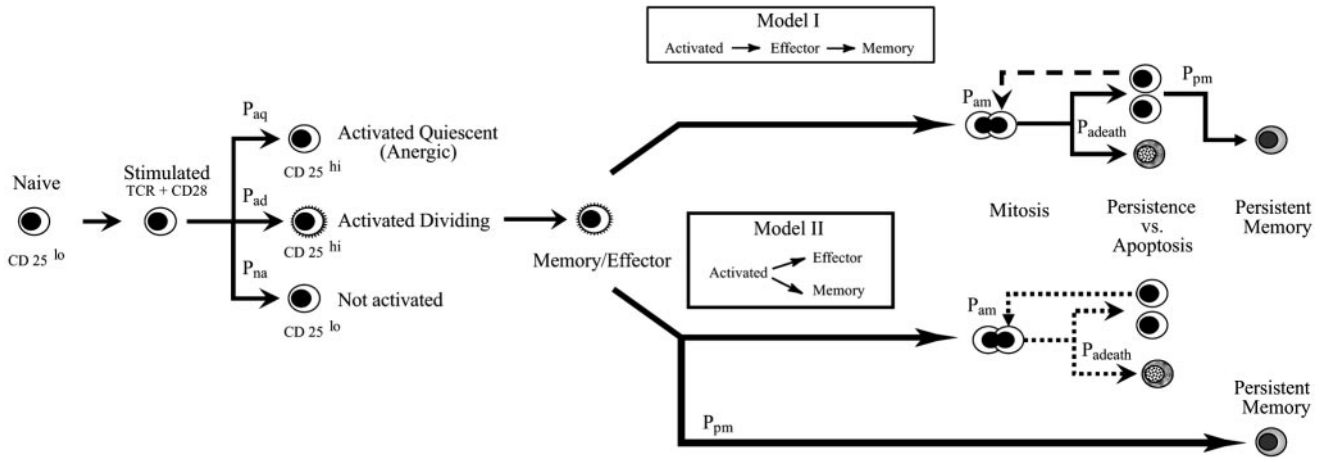

FIGURE 1. Flow diagram of the discrete event model of CD4$^+$ memory T cell emergence. Each simulation begins with each individual naive CD4$^+$ T cell undergoing an activation stimulus, and stochastically responding as an unactivated, activated nondividing (anergic), or activated dividing (effector) cell. In model I, indirect progression to the memory phenotype, memory cells arise only after progressing through several mitoses in the effector state. In model II, direct progression to memory cell status, persistent memory CD4$^+$ T cells arise directly after activation, without undergoing mitosis.

For breakpoint regression analysis, cells were stained with CDFSE and a mitotic index calculated (Fig. 3*a*). The mitotic index was defined as:

$$\sum_{i=0}^{c} \frac{n_i \times i}{T}$$

in which c = maximum number of mitoses present, i = mitotic cycle since activation, n_i = number of cells within the analysis gate for the i mitotic cycle, and T = total number of cells counted. The activation delay point was then derived by breakpoint regression analysis (Fig. 3*b*) (35). For naive CD4 cells, linear regression of the data segment after the breakpoint (61.3 h, mitotic index 0.819) yielded an intercept (mitotic index of zero) of 52.9 ± 8.4 h. Subtracting 12 h for completion of mitosis yielded an activation delay of 41 h best modeled by a log-normal distribution.

We also measured the activation delay by the method of Gett and Hodgekin (see Fig. 3, *d–f*) (5). CDFSE-labeled CD4$^+$ T cells were sampled at various times after activation with anti-CD3 and anti-CD28 (Fig. 3*d*), yielding an activation delay time of 43.9 ± 15.4 h. These data are similar to those obtained by Gett and Hodgekin (5) using anti-CD3-activated CDFSE-labeled naive CD4$^+$ murine lymphocytes and a Gaussian curve fitting regression analysis. We used these values for our simulation.

Time for completion of mitosis

The time for T cells to complete a cycle of mitosis has been estimated by various investigators from ~6 h using linear regression (36) and modeling with delay differential equations (37, 38), to up to 15.1 h using Gaussian fitting algorithm for CDFSE data and regression analysis (5). We measured mitosis time in naive human CD4$^+$ T cells activated with anti-CD3 and anti-CD28, in the presence of IL-2 by the method of Gett and Hodgekin (5) (Fig. 3*e*). The mean time to complete a cell division in this system was 12.4 ± 0.97 h, and could be modeled by either a Gaussian or log-normal curve.

Postactivation apoptosis

The magnitude of a T cell response to Ag is a balance between activation induced proliferation and apoptosis. After activation, CD4 T cells are protected at varying levels from Fas/APO1 or IL-2 withdrawal-mediated apoptosis for 6–12 division cycles (34), with memory cells having a stronger inhibition (39, 40). We derived the probability of undergoing mitosis vs apoptosis at each mitotic level. CD4$^+$ T cells were labeled with CDFSE and activated with plate-bound anti-CD3 (10 μg/ml) and anti-CD28 (10 μg/ml) in the presence of 2.5 U/ml recombinant human IL-2 (26). Cells were labeled with TOPRO-3 at various time points and analyzed by

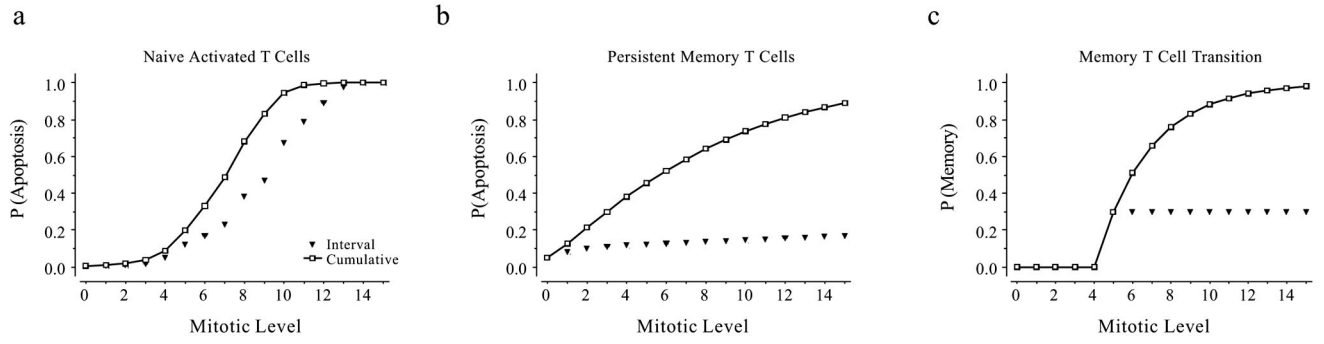

FIGURE 2. Stochastic probability distributions for apoptosis and memory cell transitions. The probability of apoptosis was specified for each post-apoptotic mitotic cycle for naive CD4$^+$ T cells (*a*), persistent memory cells (*b*), and the transition from naive to memory cell (*c*). Each plot shows the probability of apoptosis at the specified mitotic level (▼) and the cumulative probability of apoptosis for a cell progressing through successive mitoses (□).

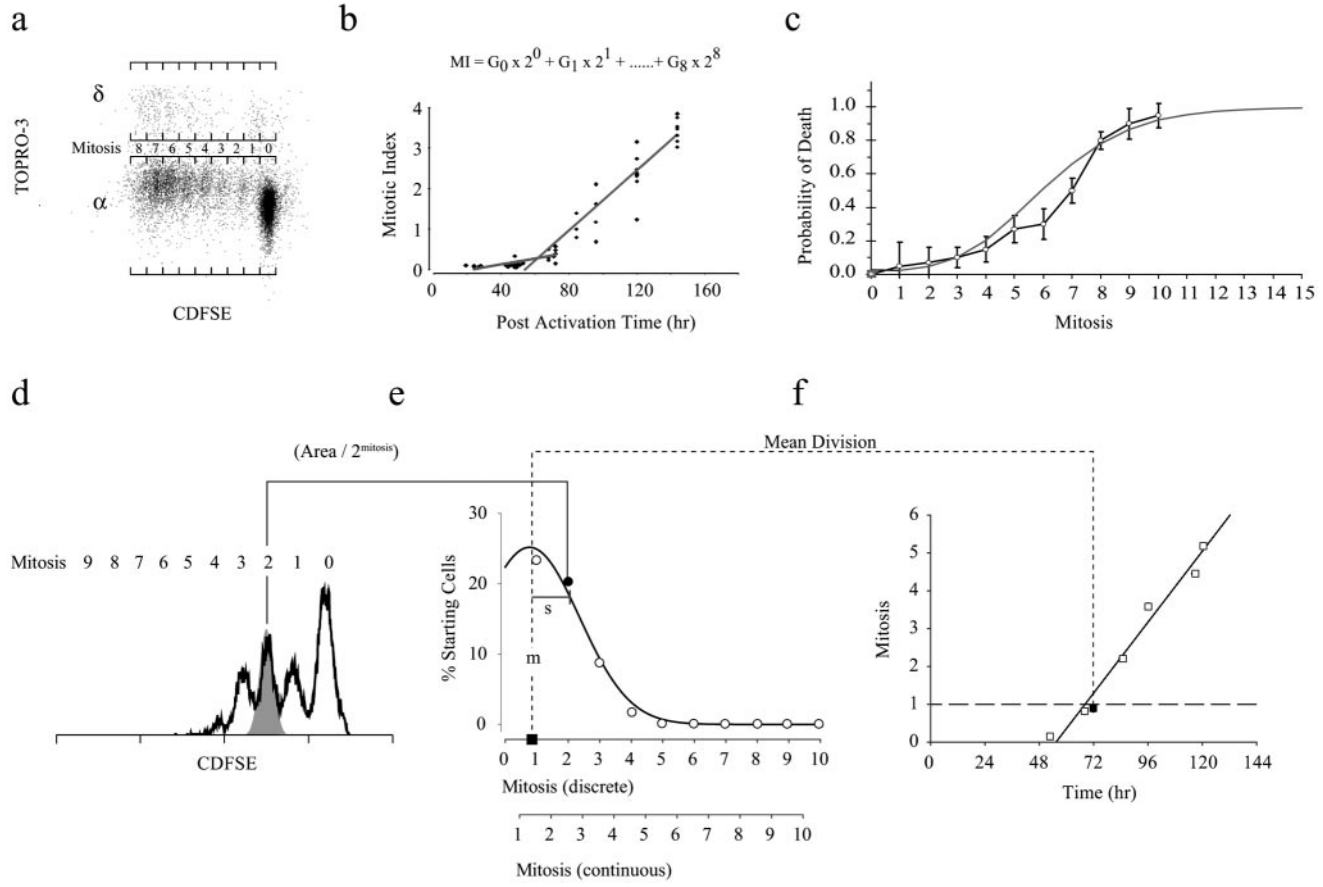

FIGURE 3. Experimental derivation of the activation delay, time to complete mitosis, and the apoptosis function for naive CD4$^+$ lymphocytes. Naive CD4$^+$ T cells were labeled with CDFSE and activated by plate-adsorbed anti-CD3 (10 μg/ml) and anti-CD28 (10 μg/ml) in the presence of 20 U/ml recombinant human IL-2. *a*, Gating of live (α; TOPRO-3$^-$) and dead (δ; TOPRO-3$^-$) cells for calculation of the mitotic index and apoptosis probability curves. *b*, The mitotic index of CD4$^+$ naive T cells plotted over time. Lines indicate the best-fit linear regression curves derived from breakpoint analysis, with the mean time to the first G_0-S transition being 47.1 h. *c*, The death vs mitosis curve for activated naive CD4$^+$ T cells was determined by CDFSE and TOPRO-3 staining based on gating shown in *a* by the formula as found in *Results*, in which *m* is the maximum number of mitoses that can be discerned in the CDFSE profile. The complete derivation of this formula is given in *Results*. The solid line shows the sigmoid curve fitted to the data ($r = 0.6713$). Data points are for three independent experiments and error bars are mean ± SD. *e*, The time to complete a mitosis and the time to the first G_0-S transition were measured by the method of Gett and Hodgekin (5). At various time points (52, 70, 72, 80, 92, 100, and 112 h) after activation, CDFSE curves were fitted to log-normal Gaussian curves (gray histogram) to determine the proportion of cells in each division, which were then divided by 2^i (where *i* is the mitosis number) and normalized to give a total of 100%. *f*, Values for one or more divisions were fitted to a Gaussian curve to give the mean (μ) and SD (σ). *g*, The mean mitosis (μ) was plotted vs time after activation. Least-squares linear regression was used to derive the slope of the line, the inverse of which gave the mean time for cell division (t_{div}) of 12.4 ± 0.97 h. The mean activation delay time was calculated as the *x*-intercept (mitosis = 0; 56.3 h) minus the mean cell division time, yielding 43.9 h (SD of σt_{div} = 15.4 h) which was comparable to that found with breakpoint analysis in *b*.

FACS. At 96 h, seven to nine mitotic peaks were present in most samples.

We then derived a formula to calculate the probability of a cell undergoing apoptosis after undergoing *x* rounds of mitosis from FACS measurements. Assume that a set of lymphocytes is labeled with CDFSE, allowed to divide, stained with TOPRO-3 to identify dead cells, and then analyzed by FACS (Fig. 3*a*). The number of cells having undergone *i* successive divisions can be enumerated by the CDFSE gating, such that for mitotic level *i* selected by gating, α_i = the number of TOPRO-3 negative (live) cells and δ_i = the number of TOPRO-3-positive (dead) cells. A simple calculation of the percentage of dead cells at mitosis *x* is:

$$p_x = \frac{\delta_x}{\alpha_x + \delta_x} \tag{1}$$

However, this first approximation neglects cells that were alive at mitosis *x* and have gone on to further divisions to be either alive ($\alpha_{>x}$) or dead ($\delta_{>x}$). The precursors of these cells need to be counted in the denominator. The number of precursors giving rise to cells after mitosis *x* is calculated by:

$$\sum_{i=x+1}^{m} \frac{\alpha_i + \delta_i}{2^{i-x}} \tag{2}$$

in which *m* is the maximum number of mitoses that can be observed in the FACS data. Factoring these precursors into Equation 1 gives:

$$p_x = \frac{\delta_x}{\alpha_x + \delta_x + \sum_{i=x+1}^{m} \frac{\alpha_i + \delta_i}{2^{i-x}}} = \frac{\delta_x}{\sum_{i=x}^{m} \frac{\alpha_i + \delta_i}{2^{i-x}}} \tag{3}$$

Equation 3 was used to calculate the individual probabilities for cell death at each mitotic level from three independent experiments. Probabilities for mitoses 10–15 were extrapolated by fitting the curve to a sigmoid distribution. The combined measured and

Table I. *Parameter values for simulations*

Parameter	Value	Explanation	References for Methods and Values
Initial Population	10^1–10^7	Because model is scalable, a convenient starting size of 1000 cells is used.	
Responder			
Probability of becoming an activated dividing cell (P_{aq})	60% of activated cells	Defined as $CD4^+$ T cells that express CD25 after TCR ligation and divide. We verified this figure experimentally (see *Results*).	Ref. 49
Activation delay	43.9 ± 15.4 h	The delay in mitotic activity after initial TCR ligation.	Ref. 53 Ref. 5 Fig. 3
Mitosis time	12.4 ± 0.97 h	Derived from CFSE staining results (Ref. 26) and verified in our laboratory.	Ref. 5 Fig. 3
Apoptotic frequency (P_{adeath})	See Fig. 3*c*	Cell has a specific chance of apoptosis after each level of mitosis. According to a death curve.	Fig. 3
Non-Responder			
Probability of becoming a nonresponder (P_{aq})	40% of activated cells	Cells which express CD25, but do not divide. We verified this for human cells.	Ref. 26
Apoptotic frequency	43%	Empirically set to maintain a stable, small population of nonactivated T cells.	
Mitotic frequency	57%		
Mitotic time	80 ± 15.4 h	Mitosis rate of homeostatic proliferation. Estimated from murine studies.	Ref. 14 Ref. 15
Memory cells			
Probability of becoming a memory T cell (P_{pm})	See Fig. 2*c*	Activated cells that had gone through five to eight rounds of division.	Ref. 37 Figs. 2*c* and 7
Mitotic time	72 ± 15.4 h	Memory cells have a low mitosis rate, every 3–10 days. Estimated from murine studies.	Ref. 14 Ref. 15
Apoptotic frequency	10%/mitosis	Assumed.	Fig. 3*b*

extrapolated values were used in the model for the probability of death vs mitosis for activated cells (Fig. 3*d*).

Commitment to persistent memory cell status

Emergence of the effector/memory phenotype begins with the first mitotic division after activation, when surface expression of CD44 and L-selectin are up-regulated, with CD45RB and CD69 being down-regulated (36). By the 7th mitotic event, the majority of activated $CD4^+$ lymphocytes express the memory/effector phenotype (36). Effector T cells develop the same surface phenotype as Ag-experienced memory lymphocytes, making it difficult to distinguish them by surface markers (21, 41). Studies of TCR diversity suggest that the Vβ diversity of memory cells is equivalent to that seen in the starting pool of naive cells (42), suggesting that persistent memory cells are stochastically selected from a naive precursor population (42, 43). For our initial simulations, we assumed a threshold of five prior mitoses before a transition to memory/effector phenotype could occur (Fig. 2*c*). The probability remained constant above the threshold, so that activated and dividing cells that survived nine mitotic cycles and apoptotic selections had an almost 100% chance of becoming persistent memory cells. Multiple simulations, described below, were then run varying the memory cell transition point to test how sensitive the simulation results were to this parameter.

Simulation results

Using the above parameters, we investigated the sensitivity of maximum memory/effector cell burst size to changes in the activation delay, division time, apoptosis vs mitosis probabilities, memory cell transition point, and the fraction of cells becoming memory cells. Fig. 4*a* shows a basic simulation.

Scalability and stochastic behavior. One of the important properties of the model is that it is scalable in that the maximum memory cell burst size was 1.5 log units greater than the starting cell number over a 6 log range of starting cells. Fig. 4*b* demonstrates a series of simulations starting with 10^1–10^7 initial lymphocytes plotting the number of activated and apoptotic cell numbers over time. The maximum memory cell burst size was 1.5 ± 0.12 log units higher than the starting clone size, which is in agreement with reported data (44). This scalability of the model results from the condition that state transitions are specified by probabilities and do not depend on the absolute numbers of cells present. For convenience, we performed simulations with 10^2 or 10^3 initial cells. To confirm the stochastic nature of the simulations, we "labeled" each starting cell in the simulation and then tracked all daughter cells and analyzed the fate maps of the starting precursor cells. These fate maps varied widely between simulations, as shown by three fate maps for cell number 1 from different simulation runs with identical starting conditions (Fig. 4*c*)

Sensitivity of memory cell burst size. One of the most useful aspects of this model is the ability to determine how sensitive memory/effector cell burst size is to alterations in fundamental parameters. We performed such a sensitivity analysis for each critical parameter by running triplicate simulations while changing a single parameter from the base model over the range of interest.

We first performed simulations to determine the sensitivity of the memory/effector cell burst size to changes in the time to complete a mitotic cycle, assuming that the cycle time did not vary with the number of mitoses that a cell had undergone (Fig. 5). The maximum effector (Fig. 5*a*) and memory (Fig. 5*b*) cell burst sizes, as well as the total T cell number (Fig. 5*c*), did not change significantly with variations in cell division time. Similar results were obtained when the activation delay time was altered (data not shown). Alterations in mitosis and activation delay timing simply shifted the timing of maximum memory and effector cell burst sizes, but did not affect their magnitude. In contrast, shifting the

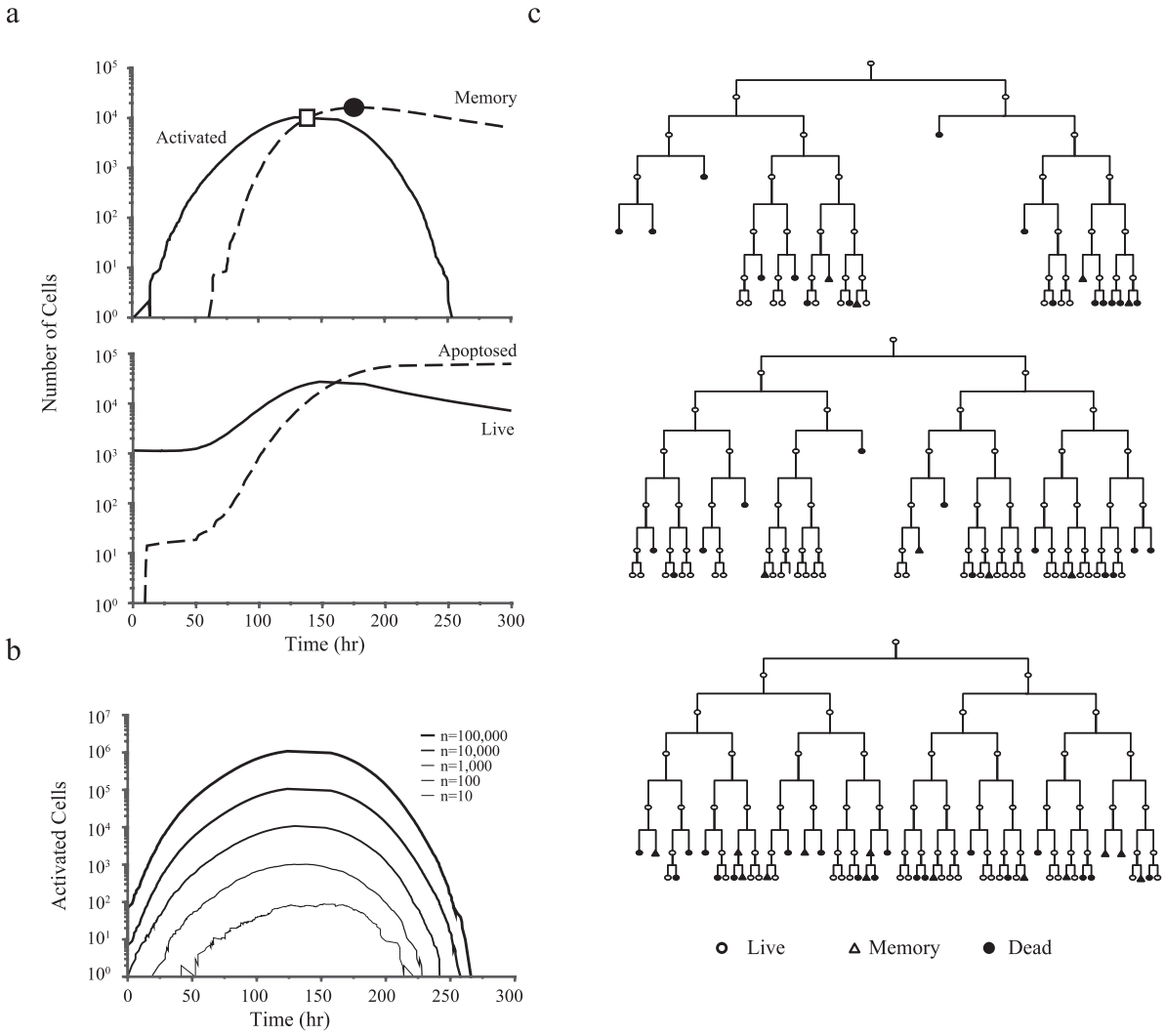

FIGURE 4. Simulation and scalability. *a*, A sample simulation with an activation delay, stochastic determination of activation delay (43.9 ± 15.4 h), and mitotic time (12.4 ± 0.98 h) showing in the upper graph the activated-dividing naive $CD4^+$ T cells (solid line) vs persistent memory cells (dashed line) and, in the lower graph the total number of viable cells (solid line) vs cumulative apoptotic cells (dashed line). Maximum burst sizes are marked for activated (□) and memory (○) cells. *b*, The model results are consistent over a wide range as demonstrated by simulations with a starting population varied over 5 logs showing total activated cells over time. *c*, The stochastic nature of the model is shown by fate mapping of the same precursor cell in three different simulations. Note that the fate of individual cell lineages varies widely, although the population-based outcomes are reproducible across different simulations.

apoptosis vs survival curve had a large effect on both memory/effector cell burst size, as well as the total number of apoptotic cells for any simulation (Fig. 6, *a* and *d*). Increasing the probability of apoptosis in early mitotic periods markedly reduced the maximum burst size and the total number of cells in the simulation.

Surprisingly, although changing the mitotic level at which cells could transition to the persistent memory type (Fig. 6, *b* and *e*) or the percentage of cells that would undergo that transition (Fig. 6, *c* and *f*) had only modest effects on memory cell burst size, these changes significantly altered the number of apoptotic cells. Shifting the mitosis number at which cells might transition to the memory phenotype to a later cycle markedly increased the percentage of cells undergoing apoptosis (Fig. 6*e*). This was a direct consequence of fewer cells being removed from the actively proliferating pool at earlier mitoses. Similarly, increasing the percentage of cells eligible to become memory cells to 50% at mitosis 5 increased the persistent memory cohort (Fig. 6, *c* and *f*). Beyond 50%, however, there was no effect.

Comparison of direct vs indirect memory cell generation

We next compared two competing hypotheses (Fig. 7) regarding the generation of persistent $CD4^+$ memory T cells: indirect emergence after progressing through an activated/effector state (model I) vs direct memory cell generation at the time of activation (model II). In model I, $CD4^+$ cells must participate in the effector burst for several mitotic cycles before they are selected to become persistent memory cells. This model is most consistent with experiments showing emergence of the memory/effector T cell phenotype after four to six mitoses (21, 36, 43, 45). In contrast, model II postulates that activated T cells are selected to become persistent memory cells immediately after activation, and do not divide or participate in the effector burst (17, 46). This model is supported by experiments showing that a subpopulation of activated T cells acquire the memory T cell phenotype without undergoing mitosis, and that virtually all cells undergo apoptosis after 6–7 postactivation mitoses (17). A

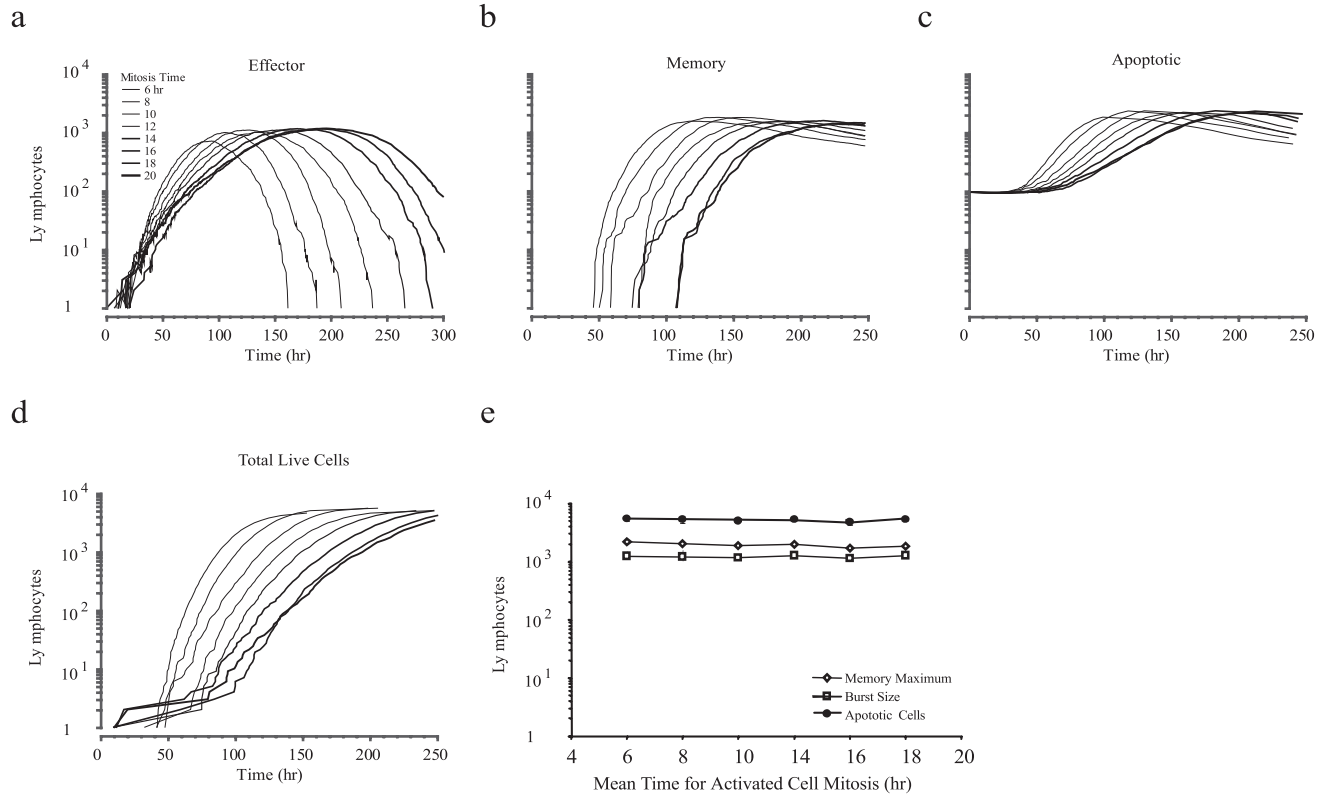

FIGURE 5. Altering the mean mitotic time does not effect burst size. To determine the sensitivity of the maximum effector (*a*) persistent memory (*b*), total viable (*c*) cell burst size, and total apoptotic (*d*) cell mass, triplicate simulations were run starting with 10^2 naive lymphocytes. Plots (*a*–*d*) show the distribution of each cell subset over time. *e*, The maximum memory, effector burst size, and apoptotic cell size are plotted against the mean mitotic cycle time demonstrating no change in these indicators over a 3-fold range of mean mitotic cycle times (6–18 h, Gaussian distribution).

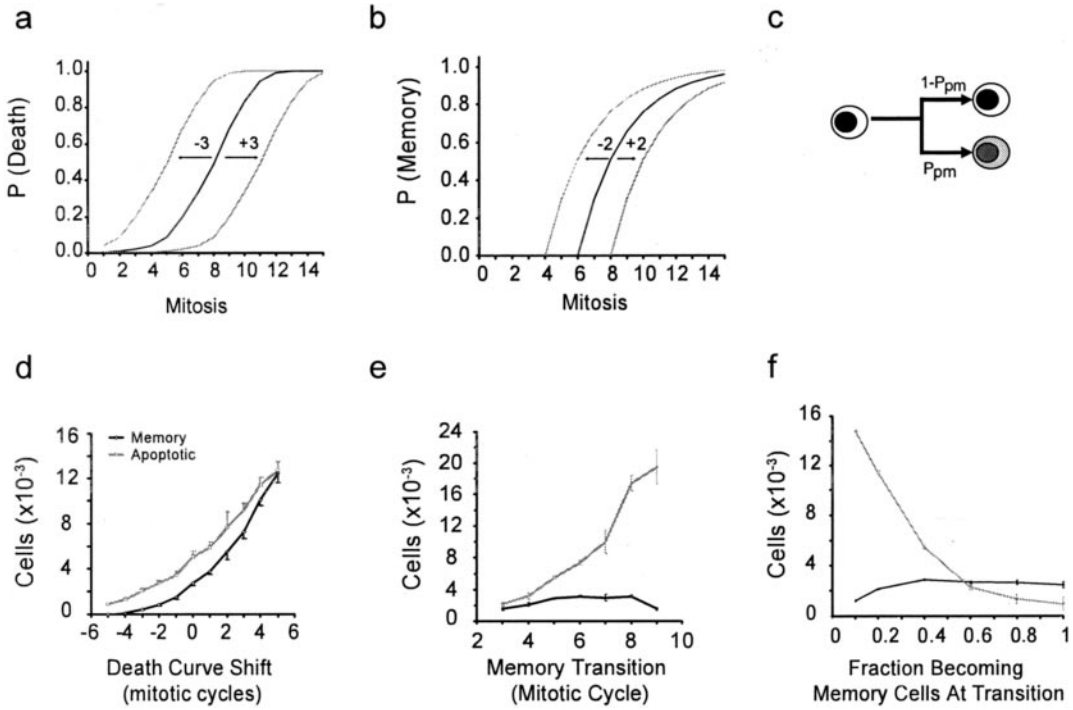

FIGURE 6. Effects of alterations in the death curve, mitotic cycle of memory cell transition, and memory cell transition fraction. The sensitivity of the memory cell burst size and total number of apoptotic cells to variations in the mitosis vs apoptosis curve (*a* and *c*), the mitotic threshold for memory cell transition in model I (*b* and *d*), and the fraction of activated cells completing the memory cell transition (*c* and *f*) at mitotic cycle 5. The maximum number of apoptotic cells was extremely sensitive to changes in all three parameters, whereas the memory cell burst size was only sensitive to changes in the death curve. All simulations were performed with 10^3 initial naive virtual lymphocytes and mean time for mitosis stochastically determined by the distribution in Fig. 3*b*. SD was <5% for all simulations.

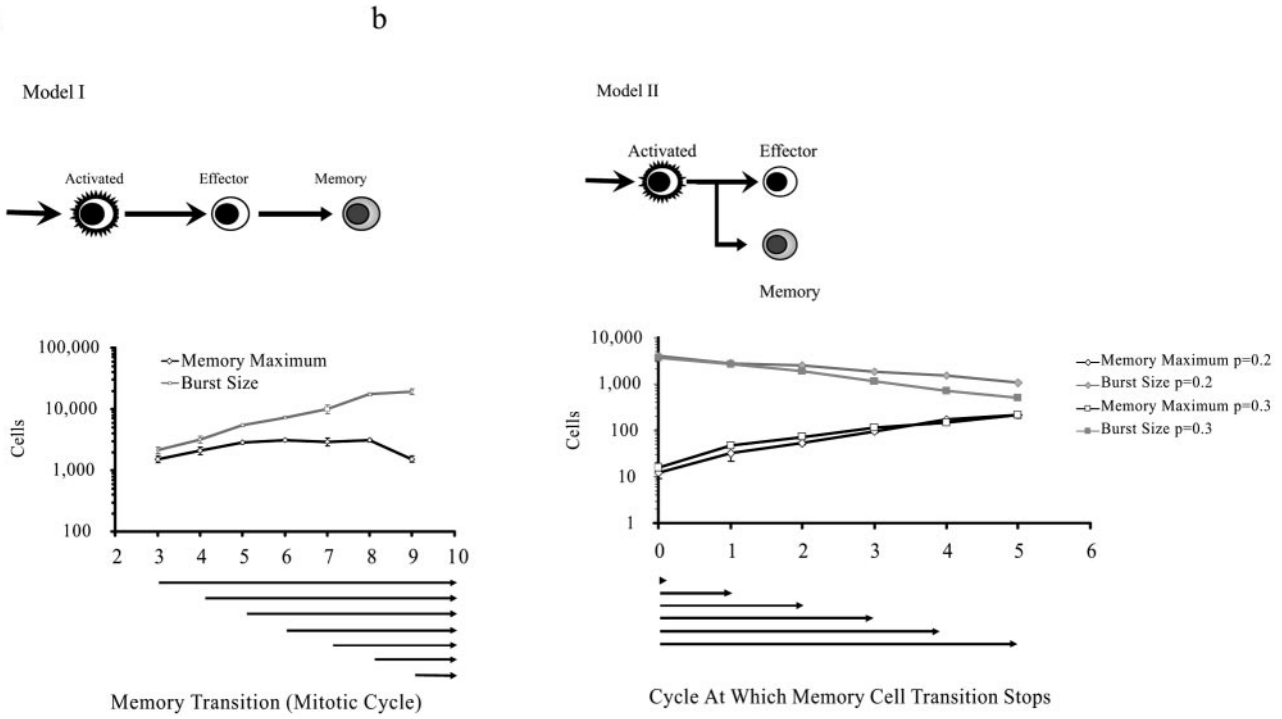

FIGURE 7. Comparison of indirect (model I) vs direct (model II) maturation of memory CD4$^+$ T cells. The memory cell burst size and maximum number of apoptotic cells were measured for model I (*a*) and model II (*b*) of memory cell maturation. Arrows below the *x*-axes depict the range of mitotic levels at which activated dividing cells could begin the stochastic state change to persistent memory cells. Model I simulations had memory burst sizes that were 0.5–2.5 log greater than those in model II simulations at all levels. Simulations were performed in triplicate with 10^2 initial naive virtual lymphocytes and mean time for mitosis stochastically determined by the distribution in Fig. 3*b*. SD was <5% for all data points.

key feature of both models is the extremely low mitotic rate of persistent memory cells, dividing every 7–21 days (13, 47).

For simulations of both models, we assumed that the frequency of memory T cell mitoses was low, 40% of memory cells undergoing mitosis every ~60 h as specified by a log-normal distribution. We used the maximum memory cell burst size as an outcome measure (Fig. 2*a*). For model I simulations (Fig. 7*a*), transition to memory phenotype was stochastically determined only after cells had progressed through at least five postactivation mitoses (threshold level). For model II simulations (Fig. 7*b*), the memory cell transition could occur before the first activation induced mitosis, and continue for a variable number of cycles.

In model I, sensitivity analysis revealed that changes in the mitotic cycle at which memory cell transition began had up to a 10-fold effect on memory cell burst size (Fig. 6, *b* and *e*). Memory cell burst size increased with the transition rate from activated to memory cell phenotype (p_m), but increasing p_m above 0.4 had no further effect (Fig. 6*f*). In contrast, model II led to early sequestration of activated cells away from the rapidly dividing effector pool into the slowly dividing memory cell pool, and markedly decreased the memory cell burst size (Fig. 7*b*). Indeed, maximum memory cell pool sizes were one to two orders of magnitude less than those seen with model II. If the memory cell decision was made during the period before the first mitosis and continuing up through the third round of mitoses, the resulting persistent memory cohort was still smaller than the starting pool of naive cells (Fig. 7*b*). The only way to increase persistent memory cells in model II was to either increase the number of mitotic levels at which cells could still transition to the persistent memory phenotype, or to allow proliferation at the rate of effector cells for one to two mitotic cycles the memory transition had occurred.

Discussion

Using discrete event computer simulation, we have identified several key variables that heavily influence effector burst size and the persistent memory pool size. These simulations closely mimic the biology of lymphocyte activation and expansion, in which mitosis vs apoptosis decisions and division times are stochastically determined by individual cells. Using discrete-event stimulation, we are able to simulate 10^2–10^8 individual lymphocytes with the underlying premise that no single simulated lymphocyte "knows" the status of any other lymphocyte in the simulation. The simulations results do not depend on global parameters, such as the total number of T cells present at any time. It is, therefore, entirely possible to simulate the kinetics of CD4$^+$ memory cell generation without invoking a global cytokine or other humoral factor that regulates the Ag-specific responder and memory T cell mass.

One might argue that our simulations were deterministic, as burst size outcomes showed small variability when the same initial conditions were used. This argument mistakes population outcomes for determinism. It is important to recognize that aggregate properties of complex systems may appear "determined" even if the behavior of all system elements is stochastic. One example of this is the relationship between Brownian motion of individual atoms and the aggregate outcome of temperature or pressure. Application of energy to a collection of molecules gives rise to predictable changes in the aggregate measures of temperature or pressure, although the spatial path of any individual atom is neither predictable nor reproducible. In our simulations, aggregate burst size was consistent between simulations but the fate any individual lymphocyte and its daughter cells was stochastic.

We found that two variables are of primary import in determining the $CD4^+$ T cell burst size: 1) the probability curve of postactivation apoptosis at each mitotic level, and 2) the mitotic level at which activated cells start and stop transitioning to the persistent memory cell pool. Other factors, such as the activation delay time and percentage of cells making the memory transition, appear to have less effect on burst size over a wide range of values. A shorter activation delay time is, however, likely to play a role in determining the rapidity of recall responses by memory cells. Several groups have reported that the time delay between activation and the first mitotic event is shorter for memory than naive T cells (32, 48, 49). Indeed, memory T cells require 10-fold shorter exposure to Ag (1 h vs 10–20 h for naive T cells) for commitment to maximal proliferation (31), likely due to preassembly of the $CD3^+$TCR complex in memory cells (29). Future discrete event simulations may shed light on the kinetics of memory recall responses compared with that of naive $CD4^+$ cells.

Our results suggest that direct memory cell emergence (model II) results in a substantially reduced memory cell pool and effector burst size, as compared with proliferation dependent memory cell emergence (model II). This finding poses some difficulties for hypotheses of direct memory cell generation (model II), as experimental results indicate the memory cell burst size is 1.5 log units greater than the initial number of naive cells, and that this number declines to 0.5–0.75 log units at 20–60 days postactivation (44). This observation is consistent with studies of telomere length indicating that, in adults, most persistent memory T cells have undergone 20–40 mitoses (50). Considered together, these data suggest that $CD4^+$ memory T cells may undergo several mitoses before entering a refractory period, or arise from both activated-naive and dividing effector cells. Clarification of this issue will require further in vivo or in vitro experiments.

One advantage of discrete event simulations is that we are able to estimate the absolute number of apoptotic cells arising from the $CD4^+$ T cell response. We found this to be informative, as in several circumstances the number of postactivation apoptotic cells varied tremendously despite minimal changes in the T cell burst size. Both in vivo and in vitro experiments are limited in their ability to measure apoptotic cell numbers over even modest periods of time. DEM techniques could be used in future experiments to estimate the post activation apoptotic cell mass for in vivo experimentation as in, for example, whole mouse $CD4^+$ cell tracking experiments (44).

To yield useful results, computer simulations of biological processes require good estimates of input parameters, and sensitivity analysis to determine how parameter variations affect the simulation results. Critical parameters in our model included the mean, SD, and statistical distributions of the activation delay time, the time for lymphocyte division, and the death vs apoptosis curves. As others have noted, these parameters are difficult to estimate using current experimental methods (5). In our model, we used TOPRO-3 labeling to estimate the proportion of cells dying at any mitotic level. This method may underestimate cell death after 72 h as dead cells in culture breakdown and may be excluded as subcellular debris by even liberal cytometry gating strategies. Further investigations should focus on more accurate methods of estimating these parameters.

Perhaps the most important aspect of this work is the use of sensitivity analysis to assess the relative importance of each parameter to the model outcomes measures. Such understanding may be more important than absolute values of results, identifying those parameters that require precise experimental data for the model to be valid, or are useful targets for altering outcomes. Although other authors have used computer based simulation to model immune events (3–5, 51, 52), sensitivity analysis has not been a feature these studies.

Finally, our current simulation does not model in detail many key features of the immune response, including homeostatic proliferation, lymphocyte trafficking, the effects of recurrent Ag stimulation, the strength of TCR and IL-2R signaling, and the effects of regulatory T cells on responders. These models are, however, easily modified to incorporate detailed mechanisms on the individual cell level, and to add further levels of complexity. In the future, simulations modeling the specific molecular and global regulatory mechanisms that guide the behavior of individual lymphocytes may prove useful in testing quantitative hypotheses of lymphocyte responses. We hope that this type of simulation can be used as a heuristic for formulating hypotheses regarding complex interactions between multiple elements of the immune system in silico before in vivo experimentation.

Acknowledgments

We thank Charles Orosz, Alan Perelson, Tim Mossman, Richard Insel, and Iñaki Sanz for helpful discussions, and Tina Pellegrin for outstanding technical support.

References

1. Morel, P. A. 1998 Mathematical modeling of immunological reactions. *Front. Biosci. 3:d338*.
2. Piper, H., S. Litwin, and R. Mehr. 1999. Models for antigen receptor gene rearrangement. II. Multiple rearrangement in the TCR: allelic exclusion or inclusion? *J. Immunol. 163:1799*.
3. Celada, F., and P. E. Seiden. 1992. A computer model of cellular interactions in the immune system. *Immunol. Today 13:56*.
4. de Boer, R. J. 2002. Mathematical models of human $CD4^+$ T-cell population kinetics. *Neth. J. Med. 60:17*.
5. Gett, A. V., and P. D. Hodgkin. 2000. A cellular calculus for signal integration by T cells. *Nat. Immunol. 1:239*.
6. Ribeiro, R. M., H. Mohri, D. D. Ho, and A. S. Perelson. 2002. In vivo dynamics of T cell activation, proliferation, and death in HIV-1 infection: why are $CD4^+$ but not $CD8^+$ T cells depleted? *Proc. Natl. Acad. Sci. USA 99:15572*.
7. Mehr, R., M. Shannon, and S. Litwin. 1999. Models for antigen receptor gene rearrangement. I. Biased receptor editing in B cells: implications for allelic exclusion. *J. Immunol. 163:1793*.
8. Albrecht-Buehler, G. 1990. In defense of "nonmolecular" cell biology. *Int. Rev. Cytol. 120:191*.
9. Ingalls, R. G. 2002. Introduction to simulation. In *2002 Winter Simulation Conference*. E. Yucesan, C.-H. Chen, J. L. Snowdon, and J. M. Charnes, eds. Association for Computing Machinery, La Jolla, p. 7.
10. Rocha, B., N. Dautigny, and P. Pereira. 1989. Peripheral T lymphocytes: expansion potential and homeostatic regulation of pool sizes and CD4/CD8 ratios in vivo. *Eur. J. Immunol. 19:905*.
11. Tanchot, C., M. M. Rosado, F. Agenes, A. A. Freitas, and B. Rocha. 1997. Lymphocyte homeostasis. *Semin. Immunol. 9:331*.
12. Goldrath, A. W. 2002. Maintaining the status quo: T-cell homeostasis. *Microbes Infect. 4:539*.
13. Jenkins, M. K., A. Khoruts, E. Ingulli, D. L. Mueller, S. J. McSorley, R. L. Reinhardt, A. Itano, and K. A. Pape. 2001. In vivo activation of antigen-specific CD4 T cells. *Annu. Rev. Immunol. 19:23*.
14. Varga, S. M., and R. M. Welsh. 1998. Stability of virus-specific $CD4^+$ T cell frequencies from acute infection into long term memory. *J. Immunol. 161:367*.
15. Tan, J. T., B. Ernst, W. C. Kieper, E. LeRoy, J. Sprent, and C. D. Surh. 2002. Interleukin (IL)-15 and IL-7 jointly regulate homeostatic proliferation of memory phenotype $CD8^+$ cells but are not required for memory phenotype $CD4^+$ cells. *J. Exp. Med. 195:1523*.
16. Lanzavecchia, A., and F. Sallusto. 2002. Progressive differentiation and selection of the fittest in the immune response. *Nat. Rev. Immunol. 2:982*.
17. Ahmadzadeh, M., S. F. Hussain, and D. L. Farber. 1999. Effector CD4 T cells are biochemically distinct from the memory subset: evidence for long-term persistence of effectors in vivo. *J. Immunol. 163:3053*.
18. Merica, R., A. Khoruts, K. A. Pape, R. L. Reinhardt, and M. K. Jenkins. 2000. Antigen-experienced CD4 T cells display a reduced capacity for clonal expansion in vivo that is imposed by factors present in the immune host. *J. Immunol. 164:4551*.
19. Farber, D. L. 1998. Differential TCR signaling and the generation of memory T cells. *J. Immunol. 160:535*.
20. Sprent, J., and D. F. Tough. 2001. T cell death and memory. *Science 293:245*.
21. Carter, L. L., and S. L. Swain. 1998. From naive to memory: development and regulation of $CD4^+$ T cell responses. *Immunol. Res. 18:1*.
22. Krishnan, S., V. G. Warke, M. P. Nambiar, H. K. Wong, G. C. Tsokos, and D. L. Farber. 2001. Generation and biochemical analysis of human effector CD4 T cells: alterations in tyrosine phosphorylation and loss of $CD3\zeta$ expression. *Blood 97:3851*.

23. Schriber, T. J., and D. T. Brunner. 2001. Inside discrete-event simulation software: how it works and why it matters. In *2001 Winter Simulation Conference*. B. A. Peters, J. S. Smith, D. J. Medeiros, and M. W. Rohrer, eds. Association for Computing Machinery, Arlington, p. 158.
24. Krahl, D., and J. S. Lamperti. 1997. A message-based discrete event simulation architecture. In *1997 Winter Simulation Conference*. S. Sandradottir, K. J. Healy, D. H. Withers, and B. L. Nelson, eds. Association for Computing Machinery, Atlanta, p. 1361.
25. Gudmundsdottir, H., A. D. Wells, and L. A. Turka. 1999. Dynamics and requirements of T cell clonal expansion in vivo at the single-cell level: effector function is linked to proliferative capacity. *J. Immunol. 162:5212*.
26. Wells, A. D., H. Gudmundsdottir, and L. A. Turka. 1997. Following the fate of individual T cells throughout activation and clonal expansion: signals from T cell receptor and CD28 differentially regulate the induction and duration of a proliferative response. *J. Clin. Invest. 100:3173*.
27. Leitenberg, D., and K. Bottomly. 1999. Regulation of naive T cell differentiation by varying the potency of TCR signal transduction. *Semin. Immunol. 11:283*.
28. Bitmansour, A. D., D. C. Douek, V. C. Maino, and L. J. Picker. 2002. Direct ex vivo analysis of human CD4$^+$ memory T cell activation requirements at the single clonotype level. *J. Immunol. 169:1207*.
29. Lanzavecchia, A., and F. Sallusto. 2000. Dynamics of T lymphocyte responses: intermediates, effectors, and memory cells. *Science 290:92*.
30. Zell, T., A. Khoruts, E. Ingulli, J. L. Bonnevier, D. L. Mueller, and M. K. Jenkins. 2001. Single-cell analysis of signal transduction in CD4 T cells stimulated by antigen in vivo. *Proc. Natl. Acad. Sci. USA 98:10805*.
31. Iezzi, G., K. Karjalainen, and A. Lanzavecchia. 1998. The duration of antigenic stimulation determines the fate of naive and effector T cells. *Immunity 8:89*.
32. Modiano, J. F., J. Mayor, C. Ball, C. G. Chitko-McKown, N. Sakata, J. Domenico-Hahn, J. J. Lucas, and E. W. Gelfand. 1999. Quantitative and qualitative signals determine T-cell cycle entry and progression. *Cell. Immunol. 197:19*.
33. Appleman, L. J., A. Berezovskaya, I. Grass, and V. A. Boussiotis. 2000. CD28 costimulation mediates T cell expansion via IL-2-independent and IL-2-dependent regulation of cell cycle progression. *J. Immunol. 164:144*.
34. Li, Q. S., S. Tanaka, R. R. Kisenge, H. Toyoda, E. Azuma, and Y. Komada. 2000. Activation-induced T cell death occurs at G_1A phase of the cell cycle. *Eur. J. Immunol. 30:3329*.
35. Hudson, D. J. 1966. Fitting segmented curves whose join points have to be estimated. *J. Am. Stat. Assoc. 61:1097*.
36. Lee, W. T., and W. J. Pelletier. 1998. Visualizing memory phenotype development after in vitro stimulation of CD4$^+$ T cells. *Cell. Immunol. 188:1*.
37. Sidorov, I. A., and A. A. Romanyukha. 1993. Mathematical modeling of T-cell proliferation. *Math. Biosci. 115:187*.
38. Baker, C. T., G. A. Bocharov, C. A. Paul, and F. A. Rihan. 1998. Modelling and analysis of time-lags in some basic patterns of cell proliferation. *J. Math. Biol. 37:341*.
39. Inaba, M., K. Kurasawa, M. Mamura, K. Kumano, Y. Saito, and I. Iwamoto. 1999. Primed T cells are more resistant to Fas-mediated activation-induced cell death than naive T cells. *J. Immunol. 163:1315*.
40. Refaeli, Y., L. Van Parijs, C. A. London, J. Tschopp, and A. K. Abbas. 1998. Biochemical mechanisms of IL-2-regulated Fas-mediated T cell apoptosis. *Immunity 8:615*.
41. Hu, H., G. Huston, D. Duso, N. Lepak, E. Roman, and S. L. Swain. 2001. CD4$^+$ T cell effectors can become memory cells with high efficiency and without further division. *Nat. Immun. 2:705*.
42. Blattman, J. N., D. J. Sourdive, K. Murali-Krishna, R. Ahmed, and J. D. Altman. 2000. Evolution of the T cell repertoire during primary, memory, and recall responses to viral infection. *J. Immunol. 165:6081*.
43. Carter, L. L., X. Zhang, C. Dubey, P. Rogers, L. Tsui, and S. L. Swain. 1998. Regulation of T cell subsets from naive to memory. *J. Immunother. 21:181*.
44. Reinhardt, R. L., A. Khoruts, R. Merica, T. Zell, and M. K. Jenkins. 2001. Visualizing the generation of memory CD4 T cells in the whole body. *Nature 410:101*.
45. Harbertson, J., E. Biederman, K. E. Bennett, R. M. Kondrack, and L. M. Bradley. 2002. Withdrawal of stimulation may initiate the transition of effector to memory CD4 cells. *J. Immunol. 168:1095*.
46. Ahmadzadeh, M., S. F. Hussain, and D. L. Farber. 2001. Heterogeneity of the memory CD4 T cell response: persisting effectors and resting memory T cells. *J. Immunol. 166:926*.
47. Bajenoff, M., O. Wurtz, and S. Guerder. 2002. Repeated antigen exposure is necessary for the differentiation, but not the initial proliferation, of naive CD4$^+$ T cells. *J. Immunol. 168:1723*.
48. Rogers, P. R., C. Dubey, and S. L. Swain. 2000. Qualitative changes accompany memory T cell generation: faster, more effective responses at lower doses of antigen. *J. Immunol. 164:2338*.
49. Wells, A. D., M. C. Walsh, D. Sankaran, and L. A. Turka. 2000. T cell effector function and anergy avoidance are quantitatively linked to cell division. *J. Immunol. 165:2432*.
50. Bernardin, F., L. Doukhan, A. Longone-Miller, P. Champagne, R. Sekaly, and E. Delwart. 2003. Estimate of the total number of CD8$^+$ clonal expansions in healthy adults using a new DNA heteroduplex-tracking assay for CDR3 repertoire analysis. *J. Immunol. Methods 274:159*.
51. De Boer, R. J., and A. S. Perelson. 1995. Towards a general function describing T cell proliferation. *J. Theor. Biol. 175:567*.
52. Perelson, A. S. 2002. Modelling viral and immune system dynamics. *Nat. Rev. Immunol. 2:28*.
53. Weinberg, A. D., M. English, and S. L. Swain. 1990. Distinct regulation of lymphokine production is found in fresh versus in vitro primed murine helper T cells. *J. Immunol. 144:1800*.